Spaceborne observations of ocean glint reflectance and modeling of wave slope distributions

F. M. Bréon[1] and N. Henriot[1]

Received 6 October 2005; revised 23 January 2006; accepted 22 February 2006; published 2 June 2006.

[1] Measurements of wind speed and direction from the NASA Scatterometer and ocean reflectance from the POLDER multi-directional radiometer are used for a quantitative analysis of the ocean glint intensity and shape. These two instruments have been flying on board the ADEOS satellite platform, which assures a very large data set of coincident measurements distributed over all oceans. The glint intensity and pattern is directly related to the wave slope probability function. The slope distribution model developed by Cox and Munk (1954) more than half a century ago, which is a function of wind speed and direction, permits an excellent fit of the observation. In particular, the modeled mean square slope is in near perfect agreement with that derived from the satellite data. The latter permit, however, a novel analysis of the deviations from a pure Gaussian slope distribution. In particular, it is shown that the skewness is a non-linear function of the wind speed. A typical glint reflectance in the specular direction is 0.2, which is therefore significantly smaller than, for instance, a typical cloud reflectance. There are large variations with the Sun zenith angle, however, that are easily accounted for with a simple formula. The glint reflectance allows an estimate of the wind speed that is highly correlated with the independent measurement from the scatterometer, with an estimated error less than 1 m s^{-1}. The multidirectional reflectance measurements from POLDER also permit the retrieval of the wind direction, albeit only in favorable conditions depending on the respective orientation of the view and wind vectors.

Citation: Bréon, F. M., and N. Henriot (2006), Spaceborne observations of ocean glint reflectance and modeling of wave slope distributions, *J. Geophys. Res.*, *111*, C06005, doi:10.1029/2005JC003343.

1. Introduction

[2] Sunglint is a major contributor to the reflectance over the oceans. Because the sea surface is smooth at the optical wavelength scale, it is a near-perfect specular reflector. The sunrays are reflected upward close to the specular direction, with an intensity and pattern that depends on the surface roughness, itself mostly controlled by wind speed and direction. The contribution of sunglint to the measured radiance is a noise for ocean color studies or the retrieval of aerosol load over the ocean [*Ignatov et al.*, 2005; *Herman et al.*, 2005]. On the other hand, the intense sunglint contribution is needed for retrieving atmospheric column of various gases such as water vapor [*Vespérini et al.*, 1999; *Kleidman et al.*, 2000] or carbon dioxide [*Crisp et al.*, 2004]. *Kaufman et al.* [2002] suggested that the sunglint could be used for estimating aerosol absorption. These remote sensing applications often require an accurate description of the sunglint pattern.

[3] The specular reflectance intensity and pattern is directly linked to the surface slope distribution. Optical methods have therefore been used for measuring the slope probability distribution function (pdf), which could then be compared to the results of hydro-dynamical modeling [*Longuet-Higgins*, 1982; *Chapron et al.*, 2000]. *Cox and Munk* [1954a, 1954b] (hereafter referred to as CM) have used airborne photographs of the Sun glitter to estimate the sea surface slope pdf. Main results of the CM work are (1) the pdf is nearly Gaussian; (2) the mean square slope is a linear function of wind speed; (3) the upwind distribution is wider than the crosswind one; (4) the distribution is slightly peaked (small and large slope are more probable than the Gaussian model); (5) the distribution is slightly skewed upwind. The observations have then been used to fit the coefficients of a Gram-Charlier expansion. Although this model has been criticized [*Wentz*, 1976; *Tatarskii*, 2003], it is still very widely used to describe the ocean surface slope distribution as well as the ocean specular reflectance. One limitation of the CM study is the relatively poor statistics, based on 29 cases distributed over 9 days, all in the same area. Several authors have suggested that the slope pdf depends on atmospheric stability [*Haimbach and Wu*, 1985; *Hwang and Shemdin*, 1988; *Shaw and Churnside*, 1997] which raises doubts about the representativeness of CM modeling for the global oceans.

[4] Other works have attempted to measure the wave slope distribution, and/or the glint reflectance angular distribution, as a function of wind vector either in the laboratory [*Long and Huang*, 1976], from an oceanic platform

[1]Laboratoire des Sciences du Climat et de l'Environnement, CEA/DSM/LSCE, Gif sur Yvette, France.

0148-0227/06/2005JC003343$09.00

[*Hwang and Shemdin*, 1988; *Su et al.*, 2002], or from aircraft measurements [*Gatebe et al.*, 2005]. Although some of these studies have found deficiencies in the CM modeling, their statistics are too poor to lead to an alternative model.

[5] The specular reflection over the ocean is a feature widely observed in satellite imagery [*Khattak et al.*, 1991]. Such data can then be used for a quantitative analysis of the sunglint and slope pdf statistics. This requires, however, the availability of coincident observations of wind vectors. *Ebuchi and Kizu* [2002] (hereafter referred to as EK) have used coincident measurements from the Geostationary GMS and vector winds from scatterometers. Their results indicate smaller mean slopes, in particular for the upwind component, and much less anisotropy than those of the CM model.

[6] In this paper, we perform a similar analysis using observations from the POLarization and Directionality of the Earth Reflectances (POLDER) and NASA Scatterometer (NSCAT) instruments both on board the Advanced Earth Observing Satellite (ADEOS-1). The multi-directional capabilities of POLDER permit an accurate identification of clear sky even in glint-contaminated areas. The coincident measurements offer a very large statistics of wind vectors and slope pdf. The mean pdf, shown as a function of wind speed, supports most of the CM conclusions. Our statistics permit the identification of variations with wind speed that could not be observed in the CM data set. We can therefore offer an alternative model that fits better the observations. Our observations allow an accurate description of the slope pdf and glint reflectance valid for the open oceans.

[7] The data and method are described in the next section. Section 3 shows the analysis of slope pdf as a function of wind speed. In section 4, we provide some statistics on the Sun glint reflectance and compare the vector wind retrievals from POLDER and NSCAT. Section 5 discusses the results and concludes.

2. Data and Methods

2.1. NASA Scatterometer Estimates of Wind Speed and Direction

[8] The NASA scatterometer (NSCAT [*Naderi et al.*, 1991]) was launched in August 1996 as part of the Advanced Earth Observing System (ADEOS) mission. NSCAT acquired vector wind data over the ice-free global oceans from mid-September 1996 until the catastrophic failure of the platform solar panel in June 1997. Although the retrieval of surface wind speeds and directions from the scatterometer measurements is based on empirical models and requires significant processing, numerous validation exercises have shown the high quality of its products. The comparison of the retrieved wind speed against a large data set of buoy observation shows a bias of 0.3 m s^{-1} and an RMS error of 1.3 m s^{-1} [*Freilich and Dunbar*, 1999]. As for the directions, the accuracy increases as the wind speed increases. A small percentage of retrievals suffer from ambiguity errors. After removal of this erroneous data, the standard deviation of the wind direction errors is 17°. In this paper, we make use of the level-2 wind vector data processed at a resolution of 50 km described by podaac (available at http://podaac.jpl.nasa.gov:2031/DATASET_DOCS/NSCAT_nsp.html, 2005). Note that the wind speed product is given for a standard height of 10 m, while the Cox and Munk model is for a height of 12.5 m s^{-1}.

2.2. POLDER Reflectance Measurements

[9] The POLDER radiometer [*Deschamps et al.*, 1994] was on board the same platform as NSCAT and acquired measurements during the same time period. POLDER measures the radiance reflected by the Earth surface and atmosphere in 8 spectral bands distributed from the blue (443 nm) to the near IR (910 nm). In this paper, we use the 865 nm band as it is the least affected by atmospheric effects and the water column contribution to the surface reflectance is negligible. A major asset of POLDER for our objective is its multi-directional capabilities. A single point on the Earth surface is observed from up to 14 directions as the satellite flies over it. We have selected all surface targets observed close to the specular direction during the mission. The same targets are seen from directions away from the glint within 3 minutes. The off-glint directions permit easy cloud detection and an estimate of the aerosol load, which is not possible when only the specular direction is available. Measurements affected by clouds were discarded from further analysis. Note that POLDER multi-directional acquisition requires about 4 minutes, so that its measurements are not coincident with those of NSCAT stricto-senso. Because no significant change in wind speed and direction is expected over the open oceans for such small delay, we assume that the two instrument measurements are coincident.

2.3. A Few Formulae

[10] We define x as the direction to the Sun. The directional surface slopes Z_x and Z_y that lead to the specular reflection to the satellite are

$$\begin{aligned} Z_x &= \frac{\partial z}{\partial x} = -(\sin\theta_s + \sin\theta_v \cos\varphi)/(\cos\theta_s + \cos\theta_v) \\ Z_y &= \frac{\partial z}{\partial y} = -(\sin\theta_v \sin\varphi)/(\cos\theta_s + \cos\theta_v) \end{aligned} \tag{1}$$

where θ_s (resp θ_v) is the Sun (resp view) zenith angle and φ is the relative azimuth. When observing the sunglint, the relative azimuth is close to 180°. Note that negative Z_x corresponds to ocean surfaces facing the Sun. The surface slope β is related to Z_x and Z_y through:

$$\tan\beta = \sqrt{Z_x^2 + Z_y^2} \tag{2}$$

The upwind and downwind components of the sea surface slope are easily derived from Z_x and Z_y:

$$\begin{aligned} Z_{up} &= Z_x \cos\phi_{wind} + Z_y \sin\phi_{wind} \\ Z_{cr} &= Z_y \cos\phi_{wind} - Z_x \sin\phi_{wind} \end{aligned} \tag{3}$$

where ϕ_{wind} is the direction upwind with respect to the Sun direction. Thus positive Z_{up} correspond to waves facing downwind, while negative Z_{up} are waves facing upwind.

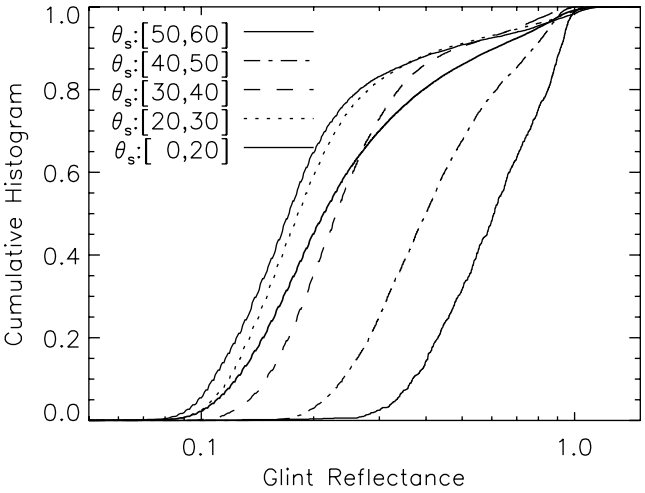

Figure 1. Cumulative histograms of measured reflectance in the specular direction. The thick line is for all suitable POLDER observations, while the various thin lines show the same for various bins of Sun zenith angle.

[11] The reflectance generated by specular reflection at the ocean surface is [*Cox and Munk*, 1954a; *Bréon and Deschamps*, 1993]:

$$R_{sp} = \frac{\pi I}{E_0 \cos\theta_s} = \frac{\pi \rho_{fr}(\theta_i)}{4 \cos\theta_s \cos\theta_v \cos^4\beta} P(Z_x, Z_y) \qquad (4)$$

where I is the reflected radiance, $E_0 \cos\theta_s$ is the solar irradiance (assumed collimated), ρ_{fr} is the Fresnel reflection coefficient, P is the wave slope probability distribution and θ_i is the incident angle which is half the phase angle:

$$\theta_i = \frac{1}{2} \cos^{-1}(\cos\theta_s \cos\theta_v + \sin\theta_s \sin\theta_v \cos\varphi) \qquad (5)$$

Note that in the specular direction ($\theta_s = \theta_v$; $\varphi = \pi$), equation (4) reduces to:

$$R_{sp} = \frac{\pi \rho_{fr}(\theta_s)}{4 \cos^2\theta_s} P(0,0) \qquad (6)$$

CM suggest to model the pdf $P(Z_{up}, Z_{cr})$ as a Gram Charlier decomposition:

$$P(Z_{up}, Z_{cr}) = \frac{1}{2\pi\sigma_{up}\sigma_{cr}} \exp\left(-\frac{\xi^2+\eta^2}{2}\right) \cdot \left\{ \begin{array}{l} 1 \\ -\frac{1}{2}c_{21}(\xi^2-1)\eta \\ -\frac{1}{6}c_{03}(\eta^3-3\eta) \\ +\frac{1}{24}c_{40}(\xi^4-6\xi^2+3) \\ +\frac{1}{24}c_{04}(\eta^4-6\eta^2+3) \\ +\frac{1}{4}c_{22}(\xi^2-1)(\eta^2-1) \end{array} \right\} \qquad (7)$$

where σ_{up} and σ_{cr} are the upwind and crosswind rms slopes, $\eta = Z_{up}/\sigma_{up}$ and $\xi = Z_{cr}/\sigma_{cr}$. The c_{ij} coefficients quantify the non-Gaussian nature of the distribution. c_{21} and c_{03} express the skewness of the upwind component, while the c_{40}, c_{04} and c_{22} coefficients describe the peakedness of the pdf. The airborne measurements in the CM study have been used to estimate these coefficients. σ_{up}, σ_{cr}, c_{21} and c_{03} were modeled as linear functions of the wind speed, while the other coefficients, barely above measurement error, are set constant.

2.4. Data Processing

[12] After cloud detection and rejection, POLDER reflectance measurements were corrected for molecular scattering and water vapor absorption. The later uses the concomitant water vapor column estimate derived from the ratio of the measurements at 910 and 865 nm. The off-glint measurements were then used to estimate other contributions such as aerosols and foam. When this contribution was found to be significant (i.e., a reflectance greater than 10^{-2}), the observation was discarded. On the other hand, for smaller contribution, it was subtracted from the glint observations. To account for atmospheric transmission, the corrected reflectances were then divided by 0.85, an empirical value that roughly corresponds to an aerosol optical thickness of 0.05 typical of the open oceans [*Kaufman et al.*, 2001]. The reflectances were then converted to a wave slope probability using equation (4).

[13] The location of the observation was used to get the corresponding wind vector from NSCAT. No spatial or temporal threshold is necessary as the POLDER and NSCAT measurements are nearly coincident. The Sun and POLDER view geometry were used to derive Z_x and Z_y (equation (1)), which were then converted to Z_{up} and Z_{cr} using NSCAT wind direction (equation (3)). This processing yields a consistent data set of (Z_{cr}, Z_{up}, *ws*, *P*) which may be use to fit various models of the surface pdf. Eight months of POLDER and NSCAT data provide 24000 coincident observations with one observation exactly in the specular direction. The final data set is based on the 7×7 neighboring pixels, and up to 14 different view directions for each pixel. After the removal of cloud and aerosol contaminated pixels, the data set is based on $9\ 10^6$ reflectance measurements, $6\ 10^6$ of which are significantly affected by the glint (i.e., $\tan\beta < 0.4$).

3. Results

3.1. How Bright Is the Ocean Glint?

[14] We first analyze the statistics of the glint reflectance at the specular point. Figure 1 shows cumulative histograms of POLDER corrected measurements for various ranges of Sun angle. The range of observed values is roughly between 0.07 and 1.2. The median value is about 0.2. Note that a reflectance greater than 1 is not unphysical as it is representative of a narrow solid angle, so that the reflected flux is still much smaller than the incident flux. On the other hand, there may be a few larger values not included in the statistics because they lead to a saturation of the POLDER detector. The shape of the cumulative histograms indicates that such saturations are significant for the high range of Sun angles. Saturation affects the high range of the histo-

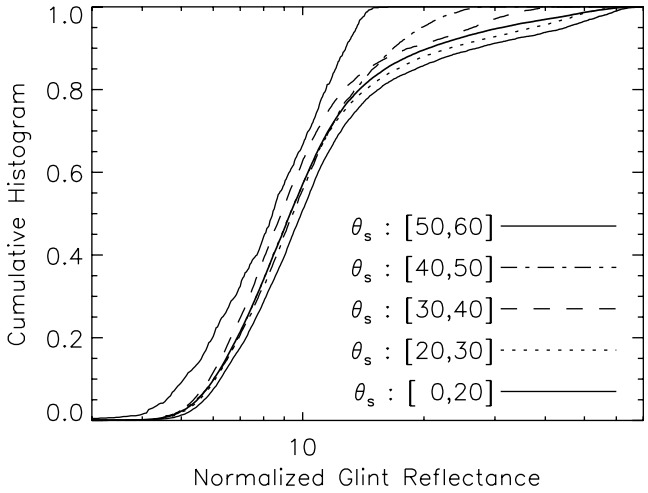

Figure 2. Same as Figure 1, but for the reflectance normalized for the Sun angle as in equation (8).

gram, which tends to shift the cumulative histogram to the left (low values). There are rather large variations of the distribution as a function of Sun angle both because of the Fresnel reflectance that increases rapidly for incidence angle greater than 40° and a $\cos^{-2}\theta_s$ dependency as shown in equation (6). This equation suggests a normalization of the reflectance in the specular direction through:

$$R_N = \frac{4\cos^2\theta_s}{\pi\,\rho_{fr}(\theta_s)} R_{sp} \tag{8}$$

Figure 2 is based on the same measurements as Figure 1 but shows the cumulative histogram of R_N. Clearly, most of the Sun geometry variability is accounted for by the normalization. The distribution of $P(0,0)$ (see equation (6)) appears mostly independent of the Sun angle, which may be expected, although some apparent correlation could have resulted from the co-variation of both variables with the latitude. Note, however, that the histogram appears slightly shifted towards low values for the largest Sun angles. This may result from the small fraction of saturated glint measurements, a case more likely for low Suns, which have been eliminated and are not included in the cumulative histograms. A typical value for R_N is 10, with 85% of the cases within a factor of 2 (i.e., between 5 and 20). This number together with equation (8) offers a typical estimate of the glint reflectance R_{sp} that accounts for the Sun geometry.

3.2. Wave Slope Distributions

[15] Figures 3 and 4 show the wave slope pdf for various ranges of wind speed. The symbols and the vertical bars indicate the mean and standard deviations of the slope probability $P(Z_{up}, Z_{cr})$ for bins of Z_{up} and Z_{cr}. The same data are shown twice on a linear and a logarithmic scale for an analysis of the behavior of the small and large values.

[16] The variability of the probability for a given slope and wind speed is rather small in comparison to its directional and wind driven variation. This observation validates the hypothesis that the slope pdf is mostly a function of wind speed and direction. Note that the variability appears much larger for the smallest wind speeds and surface slopes. This is explained in part by the large relative variation of wind speed within the bin.

[17] Although the distributions appear Gaussian at first sight, a careful analysis of Figure 3 confirms some of the CM findings. In particular, the upwind distribution appears wider than the crosswind one for wind speeds greater than 5 m s^{-1}, and this distribution is skewed towards negative slopes.

[18] The dashed line in Figures 3 and 4 corresponds to the CM model, while the plain line is the alternative model that is discussed below. Clearly, the CM model permits an excellent fit of the measurements. The measurements of the pdf appear of adequate quality to attempt a refinement of the CM model. Note also that the model fits the data rather well, down to rather infrequent slopes, over two orders of magnitudes (see Figure 4).

[19] Figure 3 is similar to the results of EK (their Figure 3), although the standard deviations obtained with POLDER measurements appear significantly smaller than those from the GMS radiometer. We offer three potential explanations: (1) the broad channel of GMS is much more affected by atmospheric scattering than the narrowband channel of POLDER at 865 nm; (2) there is no atmospheric correction in the EK study; and (3) there may be residual cloud contamination in the GMS data as it is notoriously difficult to detect clouds from a glint contaminated measurement while we use off glint POLDER observations for that purpose.

3.3. Model Fit of the Observations

[20] The rather good fit of the observations by the CM model indicates that the Gram-Charlier series, with a limited number of coefficients as in equation (7), is adequate. Our objective is to refine the coefficients of the model, and to analyze their variations with wind speed. We have therefore inverted the 7 parameters of the Gram-Charlier series (σ_{up}, σ_{cr}, c_{21}, c_{03}, c_{40}, c_{04} and c_{22}) for 30 bins of wind speed from 0 to 15 m s^{-1}. The inversion procedure minimizes the difference between the observed and modeled (as in equation (7)) probabilities. We have used the Interactive Data Language (IDL) Powell procedure for an iterative search of the minimum of the cost function. Figure 5 shows the results of the inversion for each of the 7 coefficients together with the number of observations in each wind speed bins. Note that this number is rather small for the largest wind speeds, so that the corresponding parameter estimates are probably less accurate.

Figure 3. Wave slope probability for various wind speed ranges as a function of wave slope. (left) Waves facing upwind/downwind, i.e., $|Z_{cr}| < 0.05$. (middle) Waves facing crosswind, i.e., $|Z_{up}| < 0.05$. (right) Waves facing at 45° off the wind direction, i.e., $|Z_{up} + Z_{cr}| < 0.05$ or $|Z_{up} - Z_{cr}| < 0.05$. The symbol and vertical bars indicate the mean observed probabilities and their standard deviations. The dashed and plain lines indicate the original Cox and Munk model and the corrected version.

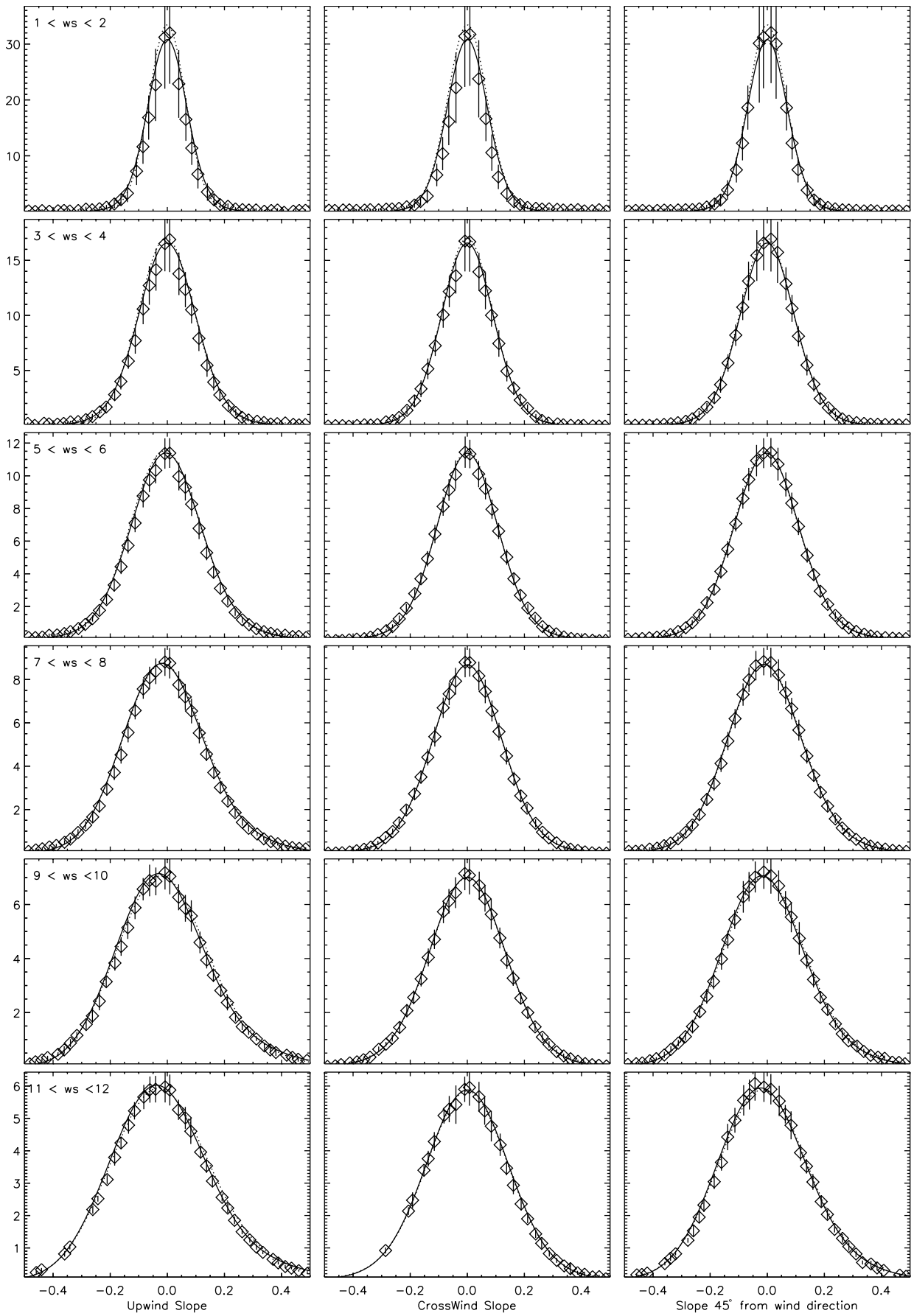
1 < ws < 2
3 < ws < 4
5 < ws < 6
7 < ws < 8
9 < ws <10
11 < ws <12
Upwind Slope
CrossWind Slope
Slope 45° from wind direction

Figure 3

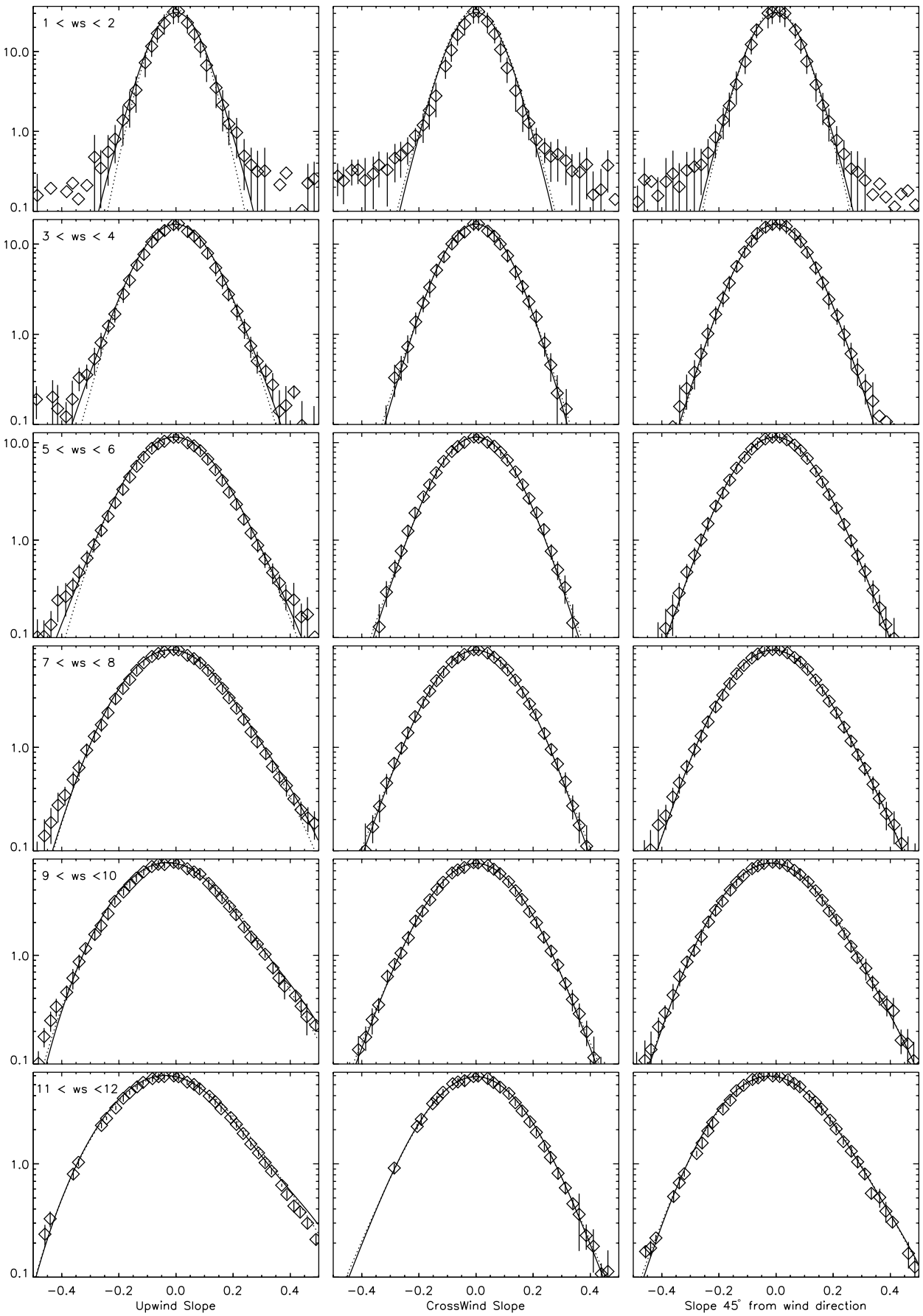

Figure 4. Same as Figure 3, but on a logarithmic scale to better depict low range values.

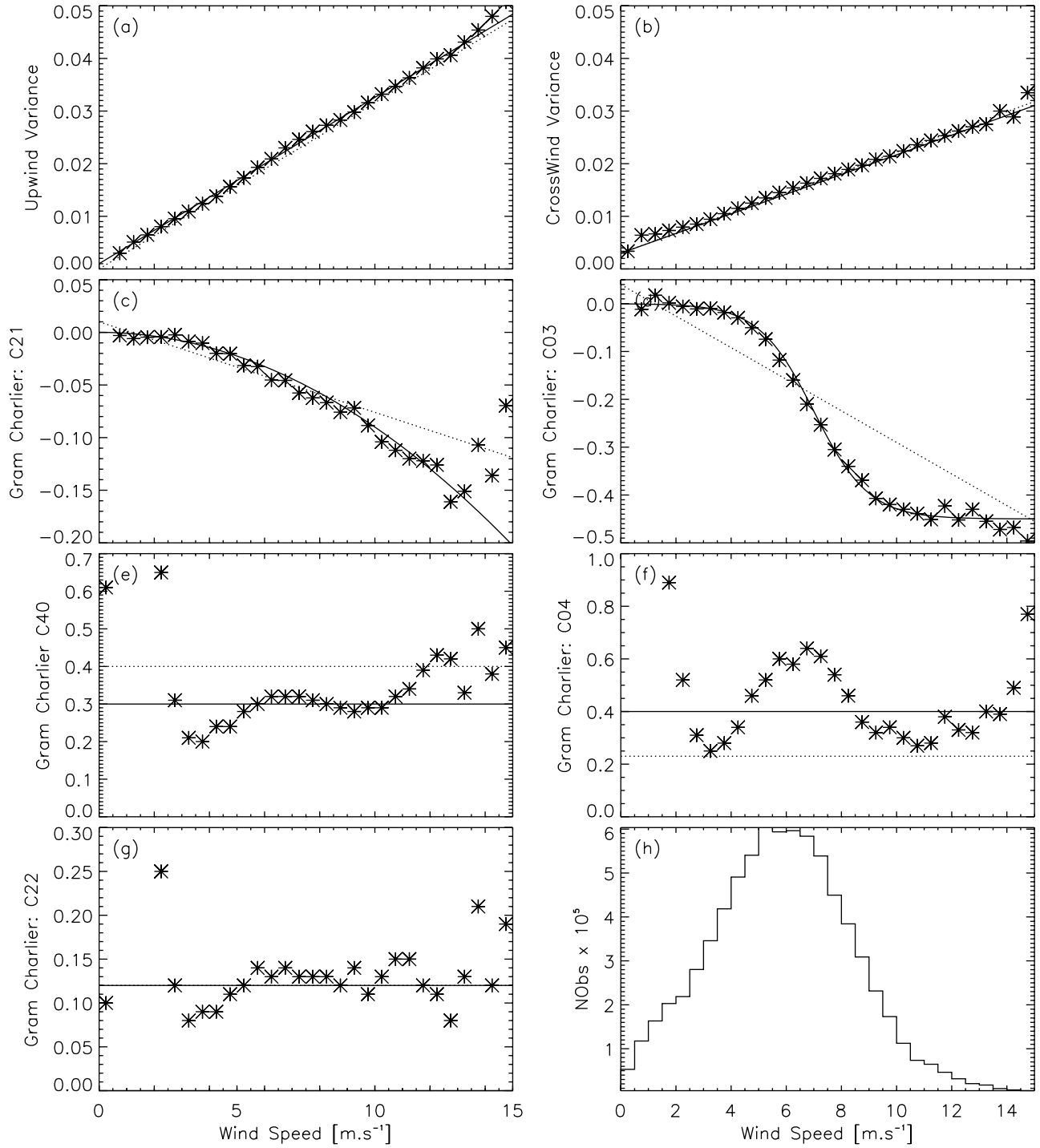

Figure 5. Retrieved parameters of the Gram-Charlier decomposition for 0.5 m s^{-1} bins of wind speed. The dashed and plain lines indicate the original Cox and Munk model and the corrected version, respectively (equation (9)). Figure 5h shows the number of measurements used for the parameter inversions.

[21] The rms slopes (σ_{up}, σ_{cr}) are shown in Figures 5a and 5b. These figures confirm the findings of CM that the mean square slopes are a linear function of wind speed and that the upwind value is generally larger than the crosswind one. There is an excellent agreement between the CM linear fit and our results, although the latter are very slightly larger, in particular for the upwind component, but well within the CM stated uncertainties. We suggest slightly different linear fits than CM, although both fits are within the variability of the measurements.

[22] The parameters c_{21} and c_{03} quantify the skewness of the distribution. Both CM and our results retrieve negative values for these parameters. This indicates that the surfaces facing upwind with a small slope are more probable than those facing downwind. The opposite is true for large slopes, which permits the necessary condition that the mean

slope is zero. The EK study did not show a skewness large enough to be extracted from the measurement variability. Our results for c_{21} clearly indicate a quadratic behavior rather than a linear one as assumed in CM. We thus suggest a different parameterization for this model parameter. On the other hand, the results for c_{03} favor neither a quadratic nor a linear behavior as assumed in CM. Empirically, we found that the variation of c_{03} is accurately fitted by a sigmoid function (see Figure 5d). This function indicates that c_{03} is close to zero for small wind speeds, and tends to saturate for wind speeds larger than 10 m s^{-1}. The other three coefficients that quantify the distribution peakedness do not show consistent variations with the wind speed. The c_{40} coefficient appears to be significantly smaller than CM best estimate while the opposite is true for c_{04}. On the other hand, the CM coefficient appears appropriate to fit our estimates of c_{22}. Interestingly, our results indicate similar values for c_{04} and c_{40} that have the same effect in the distribution for the crosswind and upwind components respectively, while CM propose a factor of 2 between the two. Note also that the measurements tend to indicate a consistent variation of c_{04} with wind speed (Figure 5f). However, there is no simple function to fit the estimates so that we chose to recommend a constant value, as for the others peakedness parameters.

[23] Our best estimates for the Gram-Charlier coefficients of equation (7) are therefore:

$$\begin{aligned}
\sigma_{up}^2 &= 10^{-3} + 3.16\ 10^{-3} ws \pm 5\ 10^{-4} \\
\sigma_{cr}^2 &= 3\ 10^{-3} + 1.85\ 10^{-3} ws\ \pm\ 5\ 10^{-4} \\
c_{21} &= -9\ 10^{-4} ws^2\ \pm\ 10^{-2} \\
c_{03} &= -0.45[1 + \exp(7 - ws)]^{-1} \pm 10^{-2} \\
c_{40} &= 0.3\ \pm\ 0.05 \\
c_{04} &= 0.4\ \pm\ 0.1 \\
c_{22} &= 0.12\ \pm\ 0.03
\end{aligned} \tag{9}$$

In equation (8), the uncertainty ranges are derived from the analysis of Figure 5 and the ability of the curve to fit the data; they have not been obtained through a proper mathematical analysis. The ability of the refined model to fit the mean pdf is shown in Figures 3 and 4 as plain lines. Both the original CM model and that proposed above fit the pdf rather well. A careful examination of Figures 3 and 4 shows a general better fit with the new model, but the improvement is subtle.

[24] We have computed several statistical coefficients to quantify the ability of the model to reproduce the probability measurement. The computation is limited to cases when the probability is larger than 0.1. The mean absolute difference is 0.41 (0.38), while the RMS difference is 1.14 (1.10) for the original (new) model. The relative error is computed as

$$err = \exp\left[\sqrt{\frac{1}{N}\Sigma\ \ln^2\left(\frac{mes}{mod}\right)}\right] - 1 \tag{10}$$

The result is 25% (22%) for the original (new) model. This error includes both the modeling error and those resulting from the uncertain estimate of wind speed and direction. It indicates that, based on a wind vector measurement from NSCAT, one can model the slope probability or the glint reflectance with a relative accuracy on the order of 25%. On the other hand, the same procedure based on ECMWF wind vectors, leads to a relative error of 35%. The comparison of the numbers show that, when modeling the glint reflectance from a numerical weather model wind field, the error is mostly due to the inaccuracy in the surface wind speed rather that an error in the surface pdf modeling.

3.4. Retrieval of Wind Speed and Direction From Optical Measurements

[25] Using either the original CM model or the refined version, a reflectance measurement may be used to estimate the wind speed. However, a single measurement is insufficient to get the effect of wind speed and atmospheric scattering on the measurements. POLDER multi-directional observation provides such opportunity. We have developed a procedure that retrieves both the wind speed and the wind direction, together with the atmospheric transmission and scattering, from the reflectance measurements. The retrieval is performed for a set of 7×7 pixels (roughly 50×50 km^2) centered on a specular observation. For each pixel, an average of 11 directions are available, some of which are affected by the glint while others are not. The off glint directions are used to detect and discard cloud contaminated pixels. The iterative retrieval procedure fits the wind speed and direction searching for the best linear correlation between the measured probability and the model. The slope of the linear fit provides an estimate of the atmospheric transmission, while the intercept corresponds to the atmospheric and foam reflectance.

[26] Figure 6 shows a bi-dimensional histogram of the POLDER and NSCAT wind speed. The symbols and bars show the mean and standard deviations of the reflectance-based estimates for 0.5 m s^{-1} bins of the wind speed retrieved by the scatterometer. There is an excellent agreement between both estimates, with a correlation of 0.93 and an RMS difference of less than 1 m s^{-1} for a large range of wind speed. We have made a similar analysis with ECMWF vector winds against both NSCAT and POLDER retrievals. The dispersion is larger with RMS differences on the order of 1.5 m s^{-1} for wind speeds between 0 and 10 m s^{-1}. The comparison of POLDER and ECMWF statistics are shown in Table 1. For wind speed less than 9 m s^{-1}, the POLDER estimates are significantly better than those from ECMWF. Clearly, the reflectance estimates benefit from the simultaneity with NSCAT. On the other hand, both Figure 6 and Table 1 show that the reflectance-based wind speed estimate is poor for wind speed larger than 10 m s^{-1}. This is likely the consequence of breaking waves and foam that partly damage the specular signature of the sea surface reflectance. Although POLDER and NSCAT are two remote sensing instruments that use the ocean surface roughness to estimate the wind speed, their principles are very different. POLDER is a passive instrument that measures sunrays at wavelengths shorter than one micron, while NSCAT is an active instrument that emits and receives at a wavelength of about 2 cm. We then argue that it is unlikely that the errors from

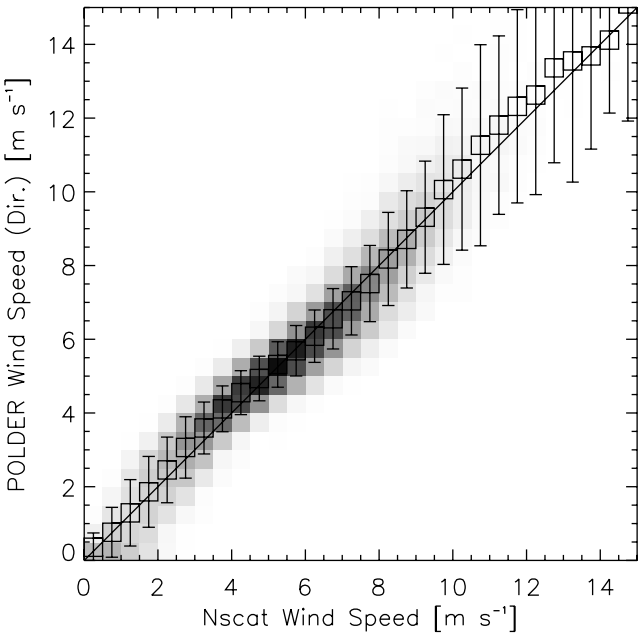

Figure 6. Bi-dimensional histogram of the wind speed derived from POLDER and NSCAT measurements. The grey scale is proportional to the number of points in each bin. The symbols and error bars indicate the mean and standard deviation of POLDER retrievals for 0.5 m s^{-1} bins of NSCAT wind speed. The statistics corresponding to this graph are shown in Table 1.

Table 1. Bias and Standard Error of Wind Speeds Derived From ECMWF Analysis and POLDER Retrievals as Compared to NSCAT Measurements[a]

NSCAT Range	Number of Cases	ECMWF		POLDER	
		Bias	Std Err	Bias	Std Err
0.0–0.5	321	2.27	1.43	0.11	0.39
0.5–1.0	532	1.8	1.35	0.01	0.66
1.0–1.5	625	1.45	1.4	0.04	0.89
1.5–2.0	826	1.19	1.51	0.11	0.95
2.0–2.5	967	0.83	1.51	0.21	0.89
2.5–3.0	1244	0.52	1.5	0.31	0.87
3.0–3.5	1464	0.29	1.51	0.34	0.77
3.5–4.0	1697	0.18	1.55	0.36	0.70
4.0–4.5	1967	−0.05	1.59	0.30	0.66
4.5–5.0	2161	−0.1	1.55	0.18	0.62
5.0–5.5	2511	−0.13	1.59	0.07	0.61
5.5–6.0	2585	−0.3	1.58	−0.06	0.68
6.0–6.5	2564	−0.45	1.58	−0.17	0.72
6.5–7.0	2618	−0.46	1.51	−0.19	0.83
7.0–7.5	2501	−0.63	1.48	−0.21	0.94
7.5–8.0	2177	−0.71	1.53	−0.24	1.05
8.0–8.5	1907	−0.76	1.48	−0.07	1.25
8.5–9.0	1613	−0.82	1.56	−0.04	1.32
9.0–9.5	1243	−0.84	1.61	0.06	1.52
9.5–10	928	−0.96	1.6	0.31	2.05
10.–10.5	669	−1.01	1.64	0.37	2.22
10.5–11	432	−1.09	1.81	0.51	2.77
11–11.5	368	−1.25	1.74	0.56	2.50
11.5–12	254	−1.35	1.88	0.57	2.69
12–12.5	173	−1.35	2.03	0.37	2.71
12.5–13	124	−1.72	2.06	0.61	2.67
13–13.5	100	−1.55	1.93	0.30	3.30
13.5–14	71	−1.74	1.76	−0.06	2.52
14–14.5	45	−1.74	1.68	−0.13	1.97
14.5–15	32	−1.73	2.79	0.34	3.18

[a]Units are in m s^{-1}.

the two estimates are correlated. Thus, both POLDER and NSCAT retrievals have an accuracy better than 1 m s^{-1} for wind speeds between 0 and 8 m s^{-1}, and on the order of 0.6 for wind speeds in the range 3–6 m s^{-1}. It is not possible to attribute the largest error to one or another. Interestingly, the statistical error derived from the comparison of satellite products is smaller than that derived from the comparison with buoys [*Freilich and Dunbar*, 1999].

[27] Figure 7 shows a comparison of the wind direction retrieved from the two instruments. A large fraction of the points are close to the 1:1 line, which demonstrates that there is wind direction information in the POLDER multi-directional measurements. On the other hand, there are also a number of retrievals with very different retrievals of wind directions. These points are concentrated along the anti-diagonal line. After investigation, we found that these retrievals suffer from ambiguity error in POLDER retrieval. When the radiometer measurements are along the crosswind direction, there is simply no information whether the wind is from the left or from the right. As a consequence, half of these cases have an erroneous direction estimate.

4. Discussion and Conclusions

[28] This paper analyses a large set of measurements of the sunglint reflectance distributed over all oceans of the Earth. The sunglint is a major feature of the bi-directional radiance field over the ocean, although a typical reflectance value at the specular point is only on the order of 0.2. The glint is therefore fainter than a typical cloud. Water bodies of smaller extension, such as lakes and ponds over land surfaces, lead to much larger specular reflectances, a consequence of smaller mean slopes than those over the oceans (F.-M. Bréon, manuscript in preparation, 2006).

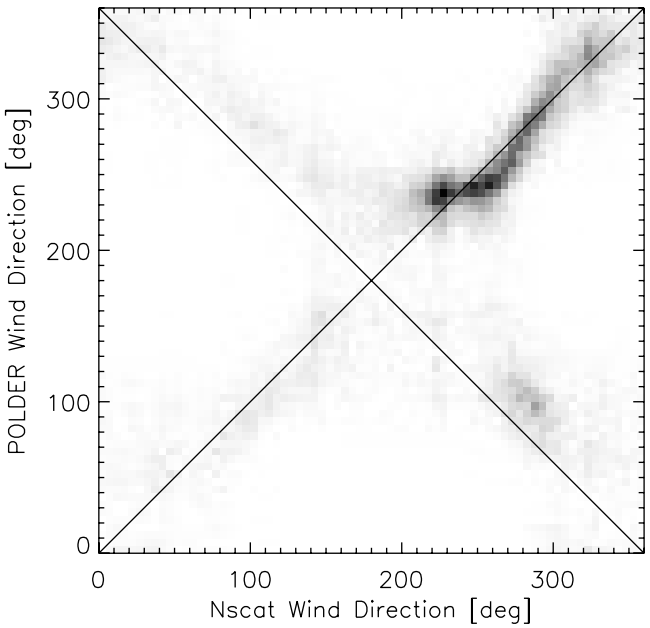

Figure 7. Bi-dimensional histogram of the wind direction derived from POLDER and NSCAT measurements. The grey scale is proportional to the number of points in each bin.

[29] The major conclusion of this work is that the Cox and Munk model of the surface slopes pdf, developed more than half a century ago from a few airborne photographs of the Sun glint, allows an amazingly accurate fit of the distributions observed from space over all oceans. The model fits the slope probability over two orders of magnitudes. In particular, the mean squared slopes, both upwind and crosswind, show a near-perfect agreement between the CM modeling and the satellite data.

[30] The very large data set of coincident wind vector and surface slope permits some refinement of the modeling, however. Our most significant finding is that the skewness coefficients, that corrects the respective probabilities of upwind and downwind slopes, follows a quadratic and sigmoid-like functions of wind speed rather than a linear form as proposed by CM. Our results also lead to different values of the peakedness coefficients, although with a variation with wind speed that is still unclear. These are refinements that have only a small impact on the pdf modeling.

[31] Using either the original CM model or the refined version, POLDER reflectance measurements can be used to estimate the surface wind speed in favorable conditions, i.e., a clear atmosphere and a suitable viewing geometry. When these conditions are met, the wind speed appears highly accurate as the RMS difference with the coincident NSCAT retrieval is better than 1 m s^{-1}. This result may also be seen as a validation of the scatterometer product as the two satellite products are fully independent. Although an instrument like POLDER (and Parasol recently launched to be part of the so called A-Train) may be used for an accurate estimate of the wind speed, a scatterometer is much better for that purpose as it is not affected by clouds, it operates both day and night, and it has less viewing geometry constrains.

[32] **Acknowledgments.** This paper is dedicated to the memory of P. Couvert, who had initiated the analysis of the glint from combined NSCAT and POLDER observations before an early death. The reflectance data used in this paper have been acquired by the CNES POLDER instrument on board the NASDA ADEOS platform. We thank the Jet Propulsion Laboratory for processing, archiving, and distributing the NSCAT products.

References

Bréon, F.-M., and P.-Y. Deschamps (1993), An analytical model for the cloud-free atmosphere/ocean system reflectance, *Remote Sens. Environ.*, *43*, 179–192.

Chapron, B., V. Kerbaol, D. Vandemark, and T. Elfouhaily (2000), Importance of peakedness in sea surface slope measurements and applications, *J. Geophys. Res.*, *105*, 17,195–17,202.

Cox, C., and W. Munk (1954a), Measurements of the roughness of the sea surface from photographs of the Sun's glitter, *J. Opt. Soc. Am.*, *44*, 838, 850.

Cox, C., and W. Munk (1954b), Statistics of the sea surface derived from Sun's glitter, *J. Mar. Res.*, *13*, 198, 227.

Crisp, D., et al. (2004), The Orbiting Carbon Observatory (OCO) mission, *Adv. Space Res.*, *34*, 700–709.

Deschamps, P.-Y., F.-M. Bréon, M. Leroy, A. Podaire, A. Bricaud, J.-C. Buriez, and G. Seze (1994), The POLDER mission: Instrument characteristics and scientific objectives, *IEEE Trans. Geosci. Remote Sens.*, *32*, 598–615.

Ebuchi, N., and S. Kizu (2002), Probability distribution of surface slope derived using Sun glitter images from geostationary meteorological satellite and surface vector winds from scatterometers, *J. Oceanogr.*, *58*, 477–486.

Freilich, M. H., and R. S. Dunbar (1999), The accuracy of the NSCAT 1 vector winds: Comparisons with National Data Buoy Center buoys, *J. Geophys. Res.*, *104*, 11,231–11,246.

Gatebe, C. K., M. D. King, A. I. Lyapustin, G. T. Arnold, and J. Redemann (2005), Airborne spectral measurements of ocean directional reflectance, *J. Atmos. Sci.*, *62*, 1072–1092.

Haimbach, S. P., and J. Wu (1985), Field trials of an optical scanner for studying sea-surface fine structures, *IEEE J. Oceanic Eng.*, *10*, 451–453.

Herman, M., J. L. Deuzé, A. Marchand, B. Roger, and P. Lallart (2005), Aerosol remote sensing from POLDER/ADEOS over the ocean: Improved retrieval using a nonspherical particle model, *J. Geophys. Res.*, *110*, D10S02, doi:10.1029/2004JD004798.

Hwang, P. A., and O. H. Shemdin (1988), The dependence of sea surface slope on atmospheric stability and swell condition, *J. Geophys. Res.*, *93*, 13,903–13,912.

Ignatov, A., P. Minnis, N. Loeb, B. Wielicki, W. Miller, S. Sun-Mack, D. Tanré, L. Remer, I. Laszlo, and E. Geier (2005), Two MODIS aerosol products over ocean on the Terra and Aqua CERES SSF data sets, *J. Atmos. Sci.*, *62*, 1008–1031.

Kaufman, Y. J., A. Smirnov, B. N. Holben, and O. Dubovik (2001), Baseline maritime aerosol: Methodology to derive the optical thickness and scattering properties, *Geophys. Res. Lett.*, *28*, 3251–3254.

Kaufman, Y. J., J. V. Martins, L. A. Remer, M. R. Schoeber, and M. A. Yamasoe (2002), Satellite retrieval of aerosol absorption over the oceans using sunglint, *Geophys. Res. Lett.*, *29*(19), 1928, doi:10.1029/2002GL015403.

Khattak, S., R. A. Vaughan, and A. P. Cracknell (1991), Sunglint and its observation in AVHRR data, *Remote Sens. Environ.*, *37*, 101–116.

Kleidman, R. G., Y. J. Kaufman, B. C. Gao, L. A. Remer, V. G. Brackett, R. A. Ferrare, E. V. Browell, and S. Ismail (2000), Remote sensing of total precipitable water vapor in the near-IR over ocean glint, *Geophys. Res. Lett.*, *27*, 2657–2660.

Long, S. R., and N. E. Huang (1976), On the variation of growth of wave slope spectra in the capillary-gravity range with increasing wind, *J. Fluid Mech.*, *77*, 209–228.

Longuet-Higgins, M. S. (1982), On the skewness of sea surface slopes, *J. Phys. Oceanogr.*, *12*, 1283–1291.

Naderi, F. M., M. H. Freilich, and D. G. Long (1991), Spaceborne radar measurements of wind velocity over the ocean: An overview of the NSCAT scatterometer system, *Proc. IEEE*, *79*, 850–866.

Shaw, J. A., and J. H. Churnside (1997), Scanning-laser glint measurements of sea-surface slope statistics, *Appl. Opt.*, *36*, 4202–4213.

Su, W., T. P. Charlock, and K. Rutledge (2002), Observation of reflectance distribution around sunglint from a coastal ocean platform, *Appl. Opt.*, *41*, 7369–7383.

Tatarskii, V. I. (2003), Multi-gaussian representation of the Cox-Munk distribution of slopes of wind-driven waves, *J. Atmos. Oceanic Technol.*, *20*, 1697–1705.

Vespérini, M., F.-M. Bréon, and D. Tanré (1999), Atmospheric water vapor content from POLDER spaceborne measurements, *IEEE Trans. Geosci. Remote Sens.*, *37*(3), 1613–1619.

Wentz, F. J. (1976), Cox and Munk's sea surface slope variance, *J. Geophys. Res.*, *81*, 1607–1608.

F. M. Bréon and N. Henriot, Laboratoire des Sciences du Climat et de l'Environnement, CEA/DSM/LSCE, 91191 Gif sur Yvette, France. (fmbreon@cea.fr)